

Origin and temperature dependence of the first direct gap of diamond

S. Logothetidis, J. Petalas, and H. M. Polatoglou

Solid State Physics Section, Department of Physics, Aristotle University of Thessaloniki, 54006 Thessaloniki, Greece

D. Fuchs

Max-Planck-Institut für Festkörperforschung, Heisenbergstrasse 1, 7000 Stuttgart 80, Germany

(Received 21 November 1991)

In this work the optical properties of natural (IIa) and *p*-type semiconducting (IIb) diamonds were studied in the neighborhood of the first direct gap, at about 7 eV, whose energy position, nature, and origin are still under debate. The complex dielectric function $\epsilon(\omega)$ of these materials was measured by means of spectroscopic ellipsometry combined with synchrotron radiation in the energy region 5–9.5 eV and the temperature range 80–800 K. The experimental results and the origin of the first direct gap of diamond were discussed with use of band-structure and dielectric-function calculations, as obtained from the linear-muffin-tin-orbitals method. The structure in the dielectric function related to the first direct gap of diamond was found to be a contribution not only of 3→5 and 4→5 transitions, as in III-V materials, but also of 3→6 and 4→6 transitions. Furthermore, the obtained $\epsilon(\omega)$ spectra were analyzed with standard analytic line shapes and the observed differences between the two diamond types in the temperature dependence of the energy position and broadening were discussed and compared with experimental and theoretical results on other III-V and group-IV materials. A temperature coefficient of $3.1(5) \times 10^{-4}$ and $2.3(5) \times 10^{-4}$ eV/K was found for the first direct gap of diamonds IIa and IIb, respectively (values larger than 5×10^{-4} eV/K reported for the other group-IV and III-V materials), which is in quite good agreement with recent calculated results. Finally, the presence of a surface oxide layer and the way it affects the dielectric function of the material, as well as the possible occurrence of a secondary reflectivity peak reported in the literature, were also commented on and discussed.

I. INTRODUCTION

Diamond is a particularly interesting material due to the simplicity of its band structure, which serves as a model for the study of the fundamental electronic structure properties of crystals. It presents electronic, optical, and mechanical properties that have made it unique for many technological applications. The recent success in depositing diamond films on nondiamond substrates by a chemical transport method¹ has revived the interest in the material properties and potential applications but also stimulated development of low-cost ways of producing synthetic diamond films from gases [especially by epitaxial growth and chemical vapor deposition (CVD) at low temperatures].² It has been realized that its properties make diamond a useful material for electronics applications. Its wide band gap, the stability at elevated temperatures, and the convenience of hosting controllable dopants (usually boron and nitrogen) allow it to operate in high-frequency, high-power, and high-temperature applications.

Diamond is also interesting from a theoretical point of view.^{3–10} It has been a test case for over 30 years, because in its classical structure the number of electrons involved in theoretical calculations is low. As a result, a variety of computational methods, first-principles calculations, and potential models,^{5–7} especially the nonlocal pseudopotential,⁴ have been performed on diamond with considerable success, in order to determine its structural and cohesive properties.

Much remains to be done in the experimental field about the optical and electronic properties of diamond. Most of the reported work has been done using reflectance measurements in the energy region 0–30 eV, from diamond samples of type I and IIa at room and lower temperatures.^{11–17} In all these optical measurements large differences were found, not only in the absolute values of the reflectivity but also in the shape and structure of the spectra, especially in the region around 7 eV. A few more works provide us with additional experimental data on diamond: Fontanella *et al.*¹⁸ studied the temperature and pressure variation of the refractive index of type-IIa diamond using capacitance techniques at audio frequencies. Himpfel, van der Veen, and Eastman¹⁹ took measurements on boron-doped IIb diamond using photon-dependent photoemission techniques. Armon and Sellschop²⁰ studied the energy loss and the Auger spectra of diamond IIa. Collins *et al.*²¹ took luminescence and optical-absorption measurements below 6 eV on a ¹³C diamond. Therefore one can notice the lack of experimental evidence on the optical properties of diamond, especially around and above the band edge, as well as a disagreement concerning the energy position of the first direct gap and its origin and the understanding of a secondary structure that was observed in the early reflectivity spectra at low temperature.

The optical properties of solids can be best described by the complex dielectric function $\epsilon(\omega)$ [$=\epsilon_1(\omega) + i\epsilon_2(\omega)$], which is associated with other measurable optical quantities (i.e., refractive index,

reflectivity, absorption coefficient) through simple equations. The observed features of the $\epsilon(\omega)$ spectra are usually attributed to interband transitions, which take place in the vicinity of critical points (CP's) in the \mathbf{k} space. Experimental investigations on diamond are made difficult by the large band gap of the material, calling for vacuum ultraviolet spectroscopies. In this work we analyze the derivative spectra of $\epsilon(\omega)$ measured in the energy region 5–10 eV using synchrotron radiation as a source, investigate the nature and origin of the observed CP's, and perform electronic structure and dielectric-function calculations. Until now many analytical expressions have been developed in an attempt to describe the dielectric function and the dispersion of the optical constants accurately. In our work we concentrate on two models. In the first one,²² the *joint density of states* (JDOS) is considered to be a sum of contributions from the main direct optical gaps. The other one^{23,24} is an improvement of the previous model and introduces the parabolic band model (PBM) to the calculations, thus describing adequately the optical spectra of group-IV elemental and III-V and II-VI compound semiconductors.

In the following section details on the experimental procedure will be presented, followed by the band-structure and dielectric-function calculations, as well as the dielectric-function modeling in Sec. III. The results and analysis of the temperature-dependence measurements will appear in Sec. IV, with discussion following in Sec. V, and conclusions in Sec. VI.

II. EXPERIMENT

In order to study the diamond properties in the energy region 5–10 eV, we performed spectroscopic ellipsometry (SE) measurements using synchrotron radiation as a source. SE is a technique that measures directly both parts of the complex dielectric function and therefore has an advantage over other experimental techniques, such as absorption and reflectivity, which measure the dielectric function indirectly. Furthermore, SE is a better suited technique, since the dielectric function rather than the reflectivity is related to the electronic structure of materials. The study of diamond at high energies requires powerful light sources in the ultraviolet region. Conventional lamps present problems in the energy range above 6 eV.¹¹ On the other hand, synchrotron radiation is an extremely powerful source in the ultraviolet region and provides an "immense" energy spectrum. Therefore the combination of SE with synchrotron radiation sources is a powerful experimental tool and ideal for the study of the optical properties of diamond above its fundamental gap, i.e., 5.5 eV.

Our spectroscopic ellipsometry measurements took place at the synchrotron radiation laboratory BESSY in Berlin. We measured two bulk diamond IIa and IIb samples using light from a 2m-Seya-Namioka monochromator. The measurements were carried out within the energy range 5.5–9.5 eV with an energy step equal to 20 meV, at an angle of incidence of 67.5° and in the temperature range from 80 to 800 K. Details concerning the ellipsometer construction and the accuracy of the sample align-

ment will be found in Ref. 25. We simply note here that the accuracy in the angle of incidence setting is calculated to be almost $<0.2^\circ$, thus limiting the accuracy of the ϵ data to about 2–3%. However, this does not modify the details of the structure present in the SE spectra.

Both diamond samples had a rectangular shape and their size was $10 \times 5 \times 1.5 \text{ mm}^3$ approximately. Their cleaning was performed by the following four stages: Heating in trichloroethylene, then in acetone, and then in methanol, at approximately 40°C for 10 min in each chemical, and finally rinsing in deionized water. This preparation process has proved to be the most efficient, in comparison to all the other methods described in the diamond literature.^{16,17,26} Accompanied with subsequent heating in high vacuum at 500°C, the above procedure improves the surface quality, as will be discussed below. After cleaning, the samples were placed neatly in the fast-entry chamber of the ellipsometer, which was pumped down by a turbo molecular pump. When the pressure became low enough, the samples were transferred to the main chamber, where the measurements took place. The vacuum there was better than 10^{-8} Torr. During the entire measurement process the vacuum was of the order 10^{-8} Torr or better, necessary to avoid the condensation of ice and oil films at low temperatures that can take place if the pressure is higher than 10^{-7} Torr.

The cooling of the samples was achieved by pouring liquid nitrogen in a specially designed cylindrical tank, a few inches above and in excellent thermal contact with the sample holder. The latter was simultaneously heated by two symmetrically located current feedthroughs and in such a way a series of low-temperature measurements could be obtained. The sample temperature was determined with a calibrated iron-Constantan thermocouple and the temperature stability was typically 3 K.

III. METHOD OF CALCULATION AND MODELING

The electronic structure of diamond is obtained by the self-consistent linear-muffin-tin-orbital method (LMTO) in conjunction with the local-density approximation (LDA). The spin-orbit coupling is not encountered in the calculations since it is very low and considered negligible. The crystalline structure of the diamond type is rather open, hence we introduce a number of empty spheres in the lattice, in order to make the structure close packed. The well-known "gap problem" that occurs when the LDA is applied to semiconductor materials is not corrected. The main effect of this problem is an almost rigid downward shift of the conduction bands.

The imaginary part of the dielectric function of diamond is calculated along lines similar to those of Ref. 27 for energies ranging up to 20 eV. The \mathbf{k} -space integration is then performed using the tetrahedron method²⁸ based on 1900 points in the irreducible part of the Brillouin zone (BZ). The resulting $\epsilon_2(\omega)$ was convoluted with a Lorentzian function with a broadening $\Gamma=25$ meV. This broadening is used to smooth the calculated dielectric function and is quite small compared to the experimental

broadening values, as will be seen below. The real part of the dielectric function is obtained through a Kramers-Kronig transformation of $\epsilon_2(\omega)$, in which for energies larger than 20 eV a tail is attached, similar to that used in Ref. 29.

We shall first describe the analysis based on the determination of the JDOS, which is applied in the vicinity of the observed critical points fairly well. This model considers the $\epsilon_2(\omega)$ as a sum of contributions from direct optical gaps. Hence the complex dielectric function around an interband transition can be described by the following analytic line shape:³⁰

$$\epsilon(\omega) = C - Ae^{i\varphi}(\omega - E + i\Gamma)^n. \quad (1)$$

The parameters of the corresponding critical point, namely, amplitude A , energy threshold E , broadening Γ , and phase angle φ , can be determined by numerical fitting of the derivative spectra of $\epsilon(\omega)$. The exponent n has the values $-\frac{1}{2}$, 0 (logarithmic), $+\frac{1}{2}$, and -1 for one-dimensional (1D), 2D, 3D, and excitonic (Exc) line shapes, respectively. We attempted to fit the first and second derivatives of the experimental $\epsilon(\omega)$ spectra instead of the $\epsilon(\omega)$ itself, so that the features under study are enhanced. The numerical calculation of the derivative spectra was obtained by using tabulated coefficients taken from the literature⁵³ to fit a polynomial of degree five to the experimental data.²⁹ By taking into account an appropriate number of points the derivative spectra can be smoothed out without any significant distortion of the line shape. From the determined optimum parameter values we receive direct information on the energy separation between the bands and the nature of the CP.

Theory predicts that, in case the observed transition is due to a single CP, the angle φ should take values that are integer multiples of $\pi/2$. That is, for a 3D CP the integer values $\varphi=0, \pi/2, \pi$, and $3\pi/2$ correspond to M_1, M_2, M_3 , and M_0 CP's, respectively; for a 2D CP the values $\varphi=0, \pi/2$, and π refer to a minimum, a saddle point, and a maximum, respectively; for an excitonic line shape, the phase angle value $\varphi=0$ corresponds to a Fano profile, i.e., the line shape that results from the interaction of a discrete excitation with a continuous background.

The second theoretical model, according to which we fitted and analyzed our experimental data in order to study the nature of the first direct gap of diamond, is the parabolic band model.^{23,24,32} This assigns to the complex dielectric function certain analytic line shapes, which depend on the type and nature (i.e., $E_{\text{ind}}, E_0, E'_0, E_1, E'_1$, or 2D, 3D, etc.) of the observed gap. We shall briefly describe the line shapes that are important to our analysis.

The E_0 and E'_0 direct gaps (and their spin-orbit split counterparts) are in most cases regarded as 3D minima (M_0 -type) CP's, whereas the E_1 and E'_1 direct gaps in the III-V compounds (together with their spin-orbit split counterparts) are usually recognized as 3D M_1 CP's. However, the latter gaps can be treated as 2D M_0 CP's, owing to the large longitudinal effective mass along the [111] direction. The contribution of these CP's to the dielectric function is of the form^{24,32}

$$\epsilon_1(\omega) - 1 = A_0[f_1(x_0) + \frac{1}{2}(\omega_0/\omega_{0S})^{3/2}f_1(x_{0S})], \quad \text{3D CP}, \quad (2)$$

$$\epsilon_1(\omega) - 1 = A_1L(x_1) + A_{1S}L(x_{1S}), \quad \text{2D CP}, \quad (3)$$

$$\epsilon_2(\omega) = A_0[f_2(x_0) + \frac{1}{2}(\omega_0/\omega_{0S})^{3/2}f_2(x_{0S})], \quad \text{3D CP}, \quad (4)$$

$$\epsilon_2(\omega) = (\pi A_1/x_1^2)H(x_1 - 1) + (\pi A_{1S}/x_{1S}^2)H(x_{1S} - 1), \quad \text{2D CP}, \quad (5)$$

where ω_i and ω_{iS} ($i=0,1$ and s denotes the spin-orbit counterpart) are the gap energies of the 2D and 3D CP's and x_i (x_{iS}) is defined by the relation $x_i = \omega/\omega_i$ ($x_{iS} = \omega/\omega_{iS}$). The amplitude A_0 is expressed as $A_0 = (4P^2/3)(2\mu^*/\omega_0)^{3/2}$, where P^2 is the average momentum matrix element, μ^* the average reduced mass of the electron-hole pair, and $H(z)$ is the Heaviside step function. The inclusion of broadening modifies the above relations in such a way that they resemble and reproduce better the experimentally observed line shapes. Namely, we replace ω with the expression $\omega + i\Gamma$, so that the factors $f_1(x)$, $f_2(x)$, and $L(x)$ of Eqs. (2)–(5) that are given in Refs. 24 and 32 become

$$f_1(x,y) = (x^2 + y^2)^{-2}(x^2 - y^2) \times [2 - F(1+x,y) - F(1-x,y)] - 2yx[F(-x-1,y) - F(x-1,y)], \quad (6)$$

$$f_2(x,y) = \frac{(x^2 - y^2)F(x-1,y) - 2yxF(-x+1,y)}{[1 + (x^2 + y^2 - 1)H(x^2 + y^2 - 1)]^2}, \quad (7)$$

and

$$L(x,y) = -(x^2 + y^2)^{-2}0.5(x^2 - y^2) \times \ln[(x^2 - y^2 - 1)^2 + 4x^2y^2] + 2yx \times \arctan[2yx/(x^2 - y^2 - 1)], \quad (8)$$

where

$$F(x,y) = \left[\frac{x + (x^2 + y^2)^{1/2}}{2} \right]^{1/2}$$

and

$$y_i = \Gamma_i/\omega_i, \quad y_{iS} = \Gamma_{iS}/\omega_{iS} \quad (i=0,1).$$

For the energy range below the indirect gap threshold we calculated the real part $\epsilon_1(\omega)$ of the dielectric function [$\epsilon_2(\omega)=0$] by means of the well-known Seelmeier formula, where the contributions from the first direct gap (7.14 eV) and the main $\epsilon_2(\omega)$ peak (12 eV) are taken into account. The coefficient values are taken from Ref. 33.

IV. RESULTS

The calculated band structure of diamond is shown in Fig. 1 along the center Γ of the Brillouin zone and high-symmetry lines in the \mathbf{k} space. The dielectric function, calculated for diamond as mentioned above, is shown in Fig. 2. It is seen that the structure in $\epsilon_2(\omega)$, which is re-

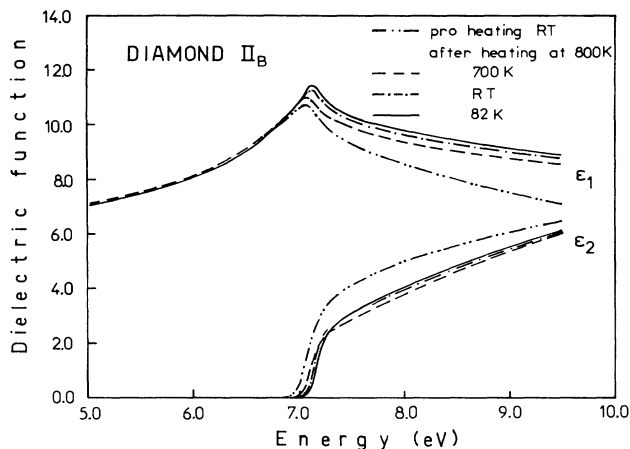


FIG. 4. The dielectric function of diamond for several temperatures, all taken after heating. The dashed-dotted line presents results at RT before heating.

have similar effects on the dielectric function. It is also notable that a rise of temperature causes a reduction of the calculated overlayer thickness.

As already pointed out, in order to improve the experimental results further, we heated the diamond IIa and IIb samples *in situ* at 500 °C for two hours and then started the temperature-dependence measurements. Typical results of the experimental dielectric function obtained after heating are shown in Fig. 3 with dashed lines at room temperature (RT).

In Fig. 4 we show the real and imaginary parts of the dielectric function of diamond IIb at 82 K (solid lines), RT (dashed-dotted lines), and 700 K (dashed lines). The main observable features are the onset of interband transitions, taking place at about 7.1 eV, the rise of $\epsilon_2(\omega)$, and the strong broad peak of $\epsilon_1(\omega)$ indicating the first direct gap of the material.

Figure 5 shows the experimental second-derivative spectra of the real (open circles) and imaginary parts (solid circles) of the dielectric function of diamond IIb with a 2D (dashes) and an excitonic (solid lines) model at 160 K.

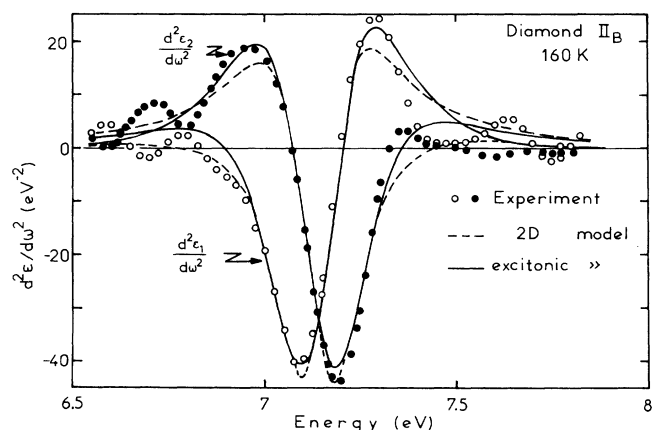


FIG. 5. Fits of the second derivatives of the real (open circles) and the imaginary (solid circles) parts of the dielectric function of diamond IIb with a 2D (dashes) and an excitonic (solid lines) model at 160 K.

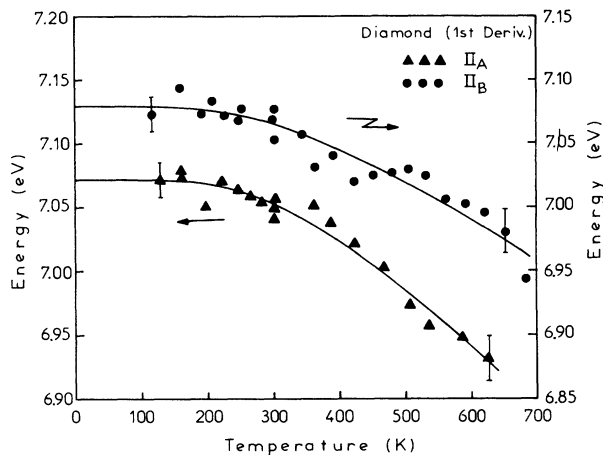


FIG. 6. Temperature dependence of the energy position of the first direct gap of diamonds IIa (triangles) and IIb (circles), as deduced from the first-derivative line-shape analysis. The solid lines represent the best fits with Eq. (9).

(solid circles) of $\epsilon(\omega)$ at 160 K in the spectral region where the first direct gap of diamond is observed. The solid and dotted lines represent the best fits to standard excitonic and 2D line shapes, respectively, derived from Eq. (1). The fit was performed simultaneously for both the real and imaginary parts of $d^2\epsilon/d\omega^2$ using a least-squares procedure. Both models have given about the same quality of fits.

In Figs. 6 and 7 we show the CP energies of both IIa and IIb diamonds obtained from the 2D line-shape analysis of the first- and second-derivative spectra of $\epsilon(\omega)$ as a function of temperature. The solid lines represent fits of the data to an average Bose-Einstein statistical factor for phonons with an average frequency Θ :^{30,36}

$$E(T) = E_B - a_B \left[1 + \frac{2}{e^{\Theta/T} - 1} \right]. \quad (9)$$

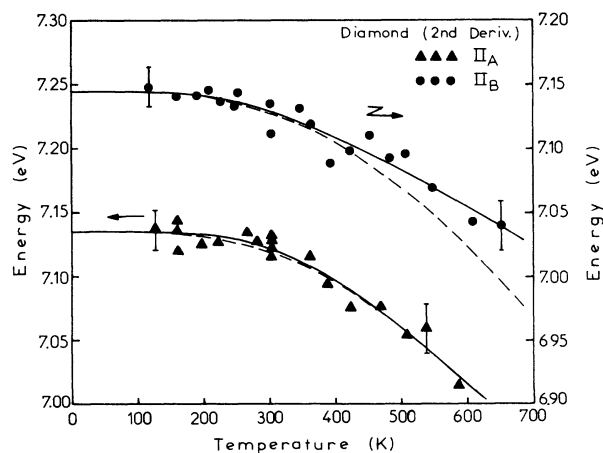


FIG. 7. Temperature dependence of the energy parameter of the first direct gap of diamonds IIa (triangles) and IIb (circles), as deduced from the second-derivative line-shape analysis. The solid lines represent the best fits with Eq. (9), while the dashed lines present theoretical results taken from Ref. 52.

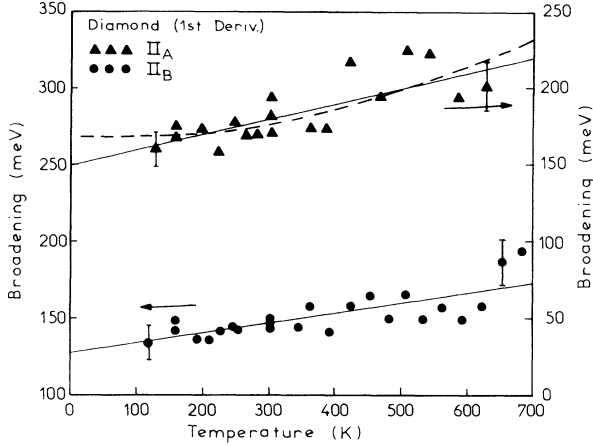


FIG. 8. Temperature dependence of the broadening parameter of the first direct gap of diamonds IIa (triangles) and IIb (circles), as deduced from the first-derivative line-shape analysis. The solid lines and dashed lines represent the best fits with Eqs. (10) and (11), respectively.

Furthermore, the temperature dependence of the broadening parameter Γ for the E'_0 gap of the IIa and IIb diamonds is shown in Figs. 8 and 9, as obtained from the first- and second-derivative spectra with 2D line-shape analysis. The dashed lines represent data fits with a formula similar to Eq. (9):

$$\Gamma(T) = \Gamma_1 + \frac{\Gamma_0}{e^{\Theta/T} - 1}. \quad (10)$$

This expression is based on the assumption of broadening by interband scattering via phonon absorption and holds only for the lowest direct gap. The parameter Γ_1 represents the broadening at zero point plus a broadening that is due to additional temperature-independent mechanisms (Auger processes, impurities, electron-electron interaction, surface scattering). The solid lines in Figs. 8 and 9 represent fits with the linear expression

$$\Gamma(T) = \Gamma_L + \gamma T. \quad (11)$$

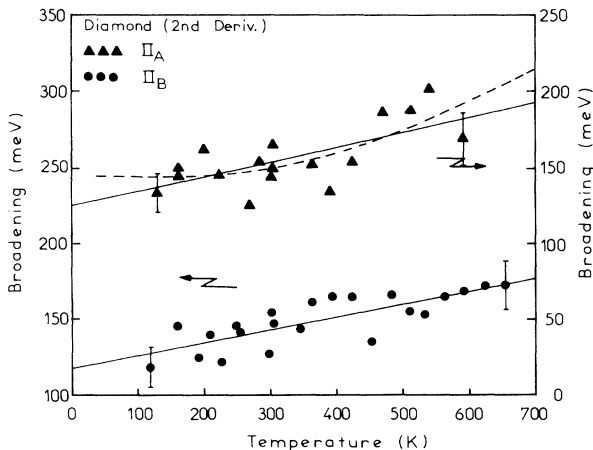


FIG. 9. As in Fig. 8, from line-shape analysis of the second-derivative spectra.

TABLE I. Values of the parameters obtained by fitting the energy gap values of the E'_0 critical point of diamonds IIa and IIb vs temperature with Eq. (9). The numbers in parentheses indicate the error margins.

	E_B (eV)	a_B (eV)	Θ (K)
Diamond IIa	7.387 (180) ^a	0.32 (18) ^a	1060 (290) ^a
	7.590 (374) ^b	0.45 (37) ^b	1300 (420) ^b
Diamond IIb	7.271 (34) ^a	0.19 (3) ^a	1000 (200) ^a
	7.322 (210) ^b	0.18 (15) ^b	970 (620) ^b

^aValues obtained by analyzing the first-derivative spectra.

^bValues obtained by analyzing the second-derivative spectra.

The values of the parameters used to describe the temperature dependence of the energy gap and broadening of the first direct gap of diamond are listed in Tables I and II, respectively, with the corresponding uncertainties representing 95% reliability.

The second theoretical model which we applied to our experimental data, in order to define the type of the first direct diamond gap, is the PBM. We performed fittings of $\epsilon_1(\omega)$ in the spectral region 6–8.3 eV, where the experimental peak is observed.

We performed fittings considering a 3D line shape but the theoretically produced peak was in most low-temperature (LT) and RT spectra blueshifted in relation to the experimental one, thus the energy gap best fit values are a bit overestimated. At RT the resulting gap energy is 6.90(5) eV, the same for both types of diamond. The broadening parameter Γ is found to be 135(25) and 115(20) meV for diamonds IIa and IIb, respectively. The overall fitting quality for diamond IIa was better than that of diamond IIb.

The consideration of two adjacent 3D+2D CP's provides fittings of the same quality, both at LT and RT. The calculations at RT have given a 2D CP lying at 7.06(3) eV and a 3D CP at 7.78(9) eV, with respective broadening parameters 235(13) and 297(45) meV and oscillator strengths 1.53(8) and 7.15(30). Thus the overall line shape of $\epsilon_1(\omega)$ results as a superposition of a 2D peak on a pronounced 3D structure. At LT the results are similar.

In Fig. 10 we show the experimental $\epsilon_1(\omega)$ data of diamond IIb at 80 K (open circles), together with the corresponding best fit line shape considering a combination of two adjacent 3D+2D CP's (solid line), as well as the two constituting CP's separately; the 3D CP is shown with the dashed-dotted line and the 2D CP with the dashes. The experimental values were fitted in the neighborhood of the observed peak (6–8.3 eV), hence the discrepancy between experiment and theory in the spectral regions 4–6 and 8.5–10 eV is well explained. The energy difference of the two adjacent CP's is estimated to be about 720 meV, hence the two CP's cannot be considered as nearly degenerate. Taking also into account that a model with two CP's involves six free parameters, whereas a model with one CP needs only three, we conclude that our PBM analysis indicates that the observed structure cannot be satisfactorily described by two neighboring 3D+2D CP's.

TABLE II. Values of the parameters obtained by fitting the broadening values of the E'_0 critical point of diamonds IIa and IIb vs temperature with Eqs. (10) and (11). The numbers in parentheses indicate the error margins.

	Γ_1 (meV)	Γ_0 (meV)	Θ (K)	Γ_L (meV)	γ (meV/K)
Diamond IIa	169 (50) ^a	212 (50) ^a	1060 (fixed) ^a	149 (21) ^a	0.108 (52) ^a
	231 (95) ^b	376 (95) ^b	1300 (fixed) ^b	125 (25) ^b	0.097 (72) ^b
Diamond IIb				127 (14) ^a	0.065 (38) ^a
				117 (14) ^b	0.086 (34) ^b

^aValues obtained by analyzing the first-derivative spectra.

^bValues obtained by analyzing the second-derivative spectra.

V. DISCUSSION

A. Nature and behavior of the first direct gap

It is generally agreed that the onset of interband transitions is due to an indirect transition between point Γ'_{25} and the absolute minimum of the conduction band, which is found along the $\langle 100 \rangle$ direction, sited approximately at (0.8,0,0). Its estimations generally coincide at about 5.49 eV.

The first direct gap of diamond lies at photon energies of about 7.1 eV. The experimental results and their theoretical interpretations about its exact position and nature are rather contradictory. The peak seems to be due to the fundamental $\Gamma'_{25}-\Gamma_{15}(E'_0)$ direct transition at the Γ point of the Brillouin zone. The first works on diamond performed reflectivity measurements in the UV region and generally agreed on the peak position: 7.1,¹¹ 7.4,¹² 7.02,¹³ about 7.2,¹⁵ and 7.3 eV,¹⁷ all measured at RT. Himpsel, van der Veen, and Eastman¹⁹ performed photon-energy-dependent photoemission measurements and located the first direct gap at 6.0(2) eV, whereas Armon and Sellschop²⁰ from electron-energy-loss-spectroscopy measurements observed it at 6.5(1.0) eV. Within the limits of the applied SE technique, we were unable to detect any structure in the energy ranges below 7 eV or higher than 7.5 eV (the latter pointed out in Ref. 16), even at LT. Therefore we propose that the main direct gap lies at photon energies at about 7.1 eV. The observed ϵ_1 peak is very pronounced. The calculations of the $\epsilon_2(\omega)$ performed in this work show that the $4 \rightarrow 5$ and $3 \rightarrow 5$ transitions are not the only band-to-band transitions that contribute to the $\epsilon_2(\omega)$, as calculated for group-IV and III-V materials for the E_1 structure,^{27,34} but that also the $4 \rightarrow 6$ and $3 \rightarrow 6$ transitions contribute significantly, since they have an early onset at the same energy. Thus the total contribution is particularly strong and the resulting peak of $\epsilon_1(\omega)$ rather sharp. Comparing the calculated $\epsilon_1(\omega)$ spectrum obtained within the one-electron calculation with the experimental one, we observe that they are in good agreement, especially because several effects, such as excitonic effects, electron-phonon interactions, and many-body corrections are not included in our calculation. Our data analysis with the PBM gave poorer results than the analysis with the JDOS model. This is due to the fact that the latter model makes use of an adjustable parameter, namely, the phase factor φ . The best fittings with the JDOS model were obtained consid-

ering a 2D line shape. The value of φ was found different than zero, which is predicted by theory for a band gap minimum M_0 . This implies³⁷ the existence of more than one nearly degenerate CP, which give a complex contribution. Our band-structure calculations (Fig. 1) show that the bands around the Γ point are rather flat and therefore transitions from an extended k region around the center of the BZ contribute at about the same energy. This fact is consistent with the calculations of $\epsilon_2(\omega)$ (Fig. 2) analyzed above. One should also note that most of the complicated structures (for example, the E_1 and E_2) observed in group-IV and III-V materials are better fitted with a 2D line shape.

Owing to the fact that the E'_0 structure of diamond is rather broad and not particularly sharp, in comparison with the corresponding peaks of other group-IV and III-V materials with lower fundamental gap, we analyzed both the first- and second-derivative spectra, in order to study the structure behavior thoroughly.

The experimental data fittings with the PBM show that a simple 3D model cannot adequately describe the first direct gap of diamond, whereas the consideration of a 2D M_1 nearby a 3D M_0 CP provides line shapes of slightly better quality. The respective gap energies are found to be 7.06 and 7.78 eV. Yet, the significant energy separa-

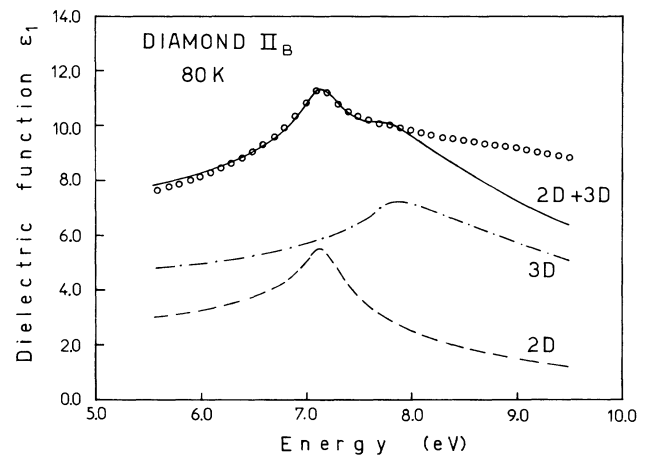


FIG. 10. Real part of the dielectric function of diamond IIb at 80 K (circles) and best fit with a 2D+3D CP line shape, as deduced from the PBM model. The dashed and dashed-dotted lines show the individual 2D and 3D CP contributions, respectively.

tion of the resulting CP's, the large difference in their amplitude values, and the overall fitting line shape cast doubts about the validity of the above consideration. Moreover, the experimental $d^2\epsilon/d\omega^2$ fittings according to the JDOS model show that the observed peak lies closer to a saddle point at all temperatures and consists of one CP.

Whether the diamond surface reconstructs by undergoing spontaneous graphitization^{38,39} or by encompassing hydrogen atoms is still under debate. Furthermore, hydrogen is in many cases the major contaminant of diamond surfaces, e.g., Cohen⁴⁰ proposed that a surface monolayer of hydrogen removes the intrinsic surface states from the gap of an otherwise clean and unreconstructed surface. Hydrogen can be chemisorbed by the diamond surface,⁴¹ especially at 900 and 1000 °C. On the other hand, oxygen seems to be another contaminant of diamond, as shown by Auger electron spectroscopy measurements,⁴² forming thin CO₂ and CO monolayers on the diamond surfaces. 5% and 0.5% oxygen monolayers were estimated after annealing at 500 and 950 °C, respectively. The formation of the above oxides and the oxygen desorption rate peaks at 500 °C (CO₂ formation) and at 550 and 800 °C (CO formation) were confirmed in Ref. 42. If one compares the experimental spectra of Fig. 4, which are taken after the heating, measured at 700 K, RT, and 82 K with those of Ref. 33 shown in Fig. 3, a difference is still observed in the dielectric function. The dashed-dotted lines in the same figure can be derived by subtracting a 5-Å-thick SiO₂ layer. This means that the hypothetical SiO₂ overlayer thickness has been reduced due to the heating.

However, it is not clear whether or not this procedure improves the measured dielectric function, especially the $\epsilon_2(\omega)$. In addition, we observed no change in the dielectric-function spectra measured in the whole temperature range after the heat treatment at 500 °C, as was the case in the preheating procedure, which supports the fact that the diamond surfaces are better after heating. This argument is further supported by the results reported in Ref. 42, according to which heating of the sample at 500 °C deforms the CO₂ layer and improves the surface. Heating at even higher temperatures causes a further improvement,⁴² but this was beyond the capabilities of our experimental setup. Nevertheless, we cannot argue whether our results or those in Ref. 33 are better. The latter have been calculated from reflectivity data (using the Kramers-Kronig relations) obtained under not so good vacuum conditions.

A second reflectivity peak was observed in Ref. 16 only at low temperatures at 7.6 eV, 0.4 eV higher than the direct E'_0 gap, and assigned to two nearly degenerate M_1 and M_2 CP's, occurring near the Γ point along the Γ - L axis. In order to explain the origin of this peak several attempts have been made. In Ref. 17 it was suggested that one CP lies along the Γ - Δ direction at energy 7.8 eV. Theoretical calculations indicate a weak structure in the range 7.6–8.4 eV,⁶ or determine a second peak at 8.22 eV (Ref. 4) (Γ_{25}^{\prime} - Γ_{15}), or 8.11 eV (Ref. 43) (Γ_{25}^{\prime} - Γ_2^{\prime}). However, our $\epsilon_2(\omega)$ calculations and analysis of the experimental data with the JDOS model show that the main direct

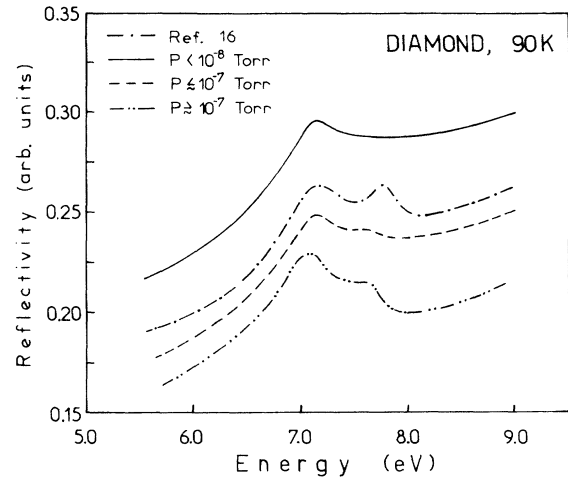


FIG. 11. Reflectivity of diamond IIb at 90 K for pressure better than 10^{-8} Torr (solid line), about 10^{-7} Torr (dashes), and worse than 10^{-7} Torr (dashed-double-dotted line). Dashed-dotted line: data from Ref. 16.

diamond gap is a complex contribution of various transitions which take place around the Γ point of the BZ and that no other gap is observed in the energy region around 7 eV.

In order to investigate the nature of the double peak that appeared in Ref. 16 we measured the dielectric function $\epsilon(\omega)$ at 80 K, when the vacuum is less than 10^{-8} Torr, a condition under which all earlier reflectivity measurements have been done. Figure 11 shows the reflectivity obtained from our dielectric-function measurements during this procedure, at three different vacuum conditions: (a) better than 10^{-8} , (b) about 10^{-7} , and (c) worse than 10^{-7} Torr. In the same figure we present the reflectivity results from Ref. 16. The double peak appears when the pressure is about 10^{-7} Torr and the second peak is more pronounced for vacuum lower than 10^{-7} Torr. By fitting the second-derivative spectra of the dielectric function with 2D line shapes, we found that the two neighboring peaks appear at [case (b)] 7.071(22) and 7.314(45) eV, with amplitudes 1.0(1) and 0.10(6), respectively, and [case (c)] 7.143(6) and 7.571(17) eV, with amplitudes 0.60(3) and 0.38(6), respectively. In case (a) the best fit was obtained considering one 2D CP, with energy position and amplitude 7.156(20) eV and 1.45(40), respectively. This result, together with the electronic structure data and the analysis of the experimental data, supports the idea that the double structure observed in Ref. 16 at low temperatures is not an intrinsic property of diamond but rather an artifact.

B. Temperature dependence of the E'_0 gap of diamond

In Tables III and IV we present the best fit values obtained by fitting the critical-point energies, which resulted considering a 2D theoretical line shape, Eq. (1), and our second-derivative experimental spectra of diamond as a function of temperature with the well-known Varshni approximation⁴⁴ and the Bose-Einstein statistical factor, Eq. (9), as well as the corresponding values of other

TABLE III. Values of E_0 , a , β , E_L , and λ of diamonds IIa and IIb, deriving from the equations $E(T)=E_0-aT^2/(T+\beta)$ and $E(T)=E_L-\lambda T$, together with other group-IV and III-V materials, all obtained from second-derivative spectra. The numbers in parentheses indicate the error margins.

	CP type	E_0 (eV)	a (10^{-4} eV/K)	β (K)	E_L (eV)	λ (10^{-4} eV/K)
Ge ^a	E_1 (2D)	2.22 (1)	6.8 (8)	240 (140)		4.8 (2)
Si ^b	E'_0 (2D)	3.354 (2)	3.5 (3.8)	580 (970)		1.7 (3)
Si ^c	E_1 (Exc)	3.457 (2)	4.7 (1.7)	350 (240)	3.486 (2)	4.1 (1)
Diamond (IIa) ^d	E'_0 (2D)	7.153 (9)	6.2 (9)	1200 (fixed)	7.216 (6)	3.1 (5)
Diamond (IIb) ^d	E'_0 (2D)	7.156 (9)	5.0 (8)	1200 (fixed)	7.185 (6)	2.3 (5)
GaAs ^e	E_0 (Exc)	1.517 (8)	5.5 (1.3)	225 (174)		3.9 (9)
GaAs ^f	E_1	3.041 (3)	7.2 (2)	205 (31)		5.2 (1)
AlAs ^g	E_0 (Exc)	2.907	8.85	313		
InP ^h	E_0					3.3 (5)
InP ⁱ	E_1 (2D)					6.0 (2)
InSb ^j	E_1 (2D)	2.00 (1)	6.84 (50)	132 (80)		6.2 (1)

^aReference 43. λ is determined in the range 100–300 K.

^bReference 44. λ is determined in the range 200–300 K.

^cReference 44. λ is determined in the range 350–800 K.

^dThis work. λ is determined in the range 200–700 K.

^eReference 29. λ is determined in the range 100–300 K.

^fReference 29. The fits have been done with an excitonic model up to 300 K and a 2D model in the temperature range from 300 to 760 K. λ is determined in the range 100–300 K.

^gReference 45.

^hReference 46. λ is determined in the range 200–300 K.

ⁱReference 46. λ is determined in the range 200–800 K.

^jReference 47. λ is determined in the range 100–700 K.

group-IV (Refs. 45 and 46) and III-V (Refs. 47–49) materials, found in the literature. It should be noted that we have taken into account only the first direct gaps of the above materials, which are of different origin in each case. Most of the group-IV and III-V materials listed in

Table III exhibit a temperature coefficient larger than or equal to 5×10^{-4} eV/K when results are taken in a wide range of temperatures. The corresponding results on diamonds IIa and IIb have lower values, around $3.1(5) \times 10^{-4}$ and $2.3(5) \times 10^{-4}$ eV/K, respectively (see

TABLE IV. Values of E_B , a_B , and Θ of diamonds IIa and IIb, deriving from Eq. (14), together with other group-IV and III-V materials, all obtained from second-derivative spectra. The numbers in parentheses indicate the error margins.

	CP type	E_B (eV)	a_B (eV)	Θ (K)
Ge ^a	E_1 (2D)	2.33 (3)	0.12 (4)	360 (120)
Si ^b	E'_0 (2D)	3.378 (16)	0.025 (17)	267 (123)
Si ^b	E_1 (Exc)	3.495 (13)	0.039 (14)	245 (62)
Diamond (IIa)	E'_0 (2D)	7.590 (374)	0.45 (30)	1300 (420)
Diamond (IIb)	E'_0 (2D)	7.322 (210)	0.18 (15)	967 (618)
GaAs ^c	E_0 (Exc)	1.571 (23)	0.057 (29)	240 (102)
GaAs ^d	E_1	3.125 (9)	0.091 (11)	274 (30)
AlAs ^e	E_0 (Exc)	3.061	0.151	400
InP ^f	E_0	1.629 (111)	0.217 (113)	697 (177)
InP ^g	E_1 (2D)	3.348 (7)	0.068 (10)	224 (30)
InSb ^h	E_1 (2D)	2.075 (50)	0.091 (30)	272 (90)

^aReference 43.

^bReference 44.

^cReference 29.

^dReference 29. The fits have been done with an excitonic model up to 300 K and a 2D model in the temperature range from 300 to 760 K.

^eReference 45.

^fReference 46. Energy gap values obtained from the ϵ_1 maxima.

^gReference 46.

^hReference 47.

Figs. 6 and 7). Diamond has a particularly large Debye temperature (2200 K), compared to other diamond-type semiconductors shown in Tables III and IV. Therefore the average phonon temperature Θ is rather high (about 1200 K), causing the E - T curves to decline slowly.

The theory for the temperature-dependence shifts has been described in Refs. 36 and 50–53. According to this theory the temperature shifts of critical points consist of three terms: the thermal expansion term, the Debye-Waller term, and the real part of the self-energy term. In a recent paper⁵⁴ the energy position of the E'_0 gap of diamond has been calculated as a function of temperature including all three contributions. In this work it was found that the shift due to thermal expansion is small, mainly due to the small pressure dependence of the E'_0 gap in diamond-type semiconductors and the large bulk modulus of diamond. On the other hand, the Debye-Waller term is dominant up to about 400 K, whereas the self-energy term is important mainly in the higher-temperature region.

The shift of the E'_0 gap as a function of temperature, which was calculated in Ref. 54 and shown with dashed lines in Fig. 5, is in quite good agreement with our results on both diamond samples, whereas a deviation is observed at temperatures higher than 500 K for diamond IIb. A temperature coefficient of 3.0×10^{-4} and $3.1(5) \times 10^{-4}$ eV/K was found from the calculated results and our results for diamond IIa, respectively, in the temperature range 200–700 K. In Ref. 13 an attempt was made in order to estimate the temperature dependence of the E'_0 gap by using the reflectivity peak at only 133 K and RT. Their estimation of the temperature coefficient is 6.05×10^{-4} eV/K, which is rather large. On the other hand, the corresponding result concerning the indirect gap of diamond, measured in the whole temperature range 135–600 K is 5×10^{-4} eV/K.

Calculations of the electron-phonon spectral functions for Si and Ge,³⁶ diamond,⁵⁴ and GaAs (Ref. 53) have shown that the acoustical as well as the optical phonons contribute to the energy shifts due to the electron-phonon interaction, whereas for the broadening mainly the optical phonons are responsible. Furthermore, the total area under the spectral function increases with increasing distance from the Γ point of the BZ, because of the increasing electronic density of states. Near the Γ point the main contribution arises from the optical phonons, hence a low Θ (average phonon frequency) indicates how large the contribution of the acoustical phonons to the broadening is. The zero-point broadening [$\Gamma(T=0)$] has been found to be by no means negligible and is proportional to the area under the spectral function. For the broadening parameter we expect an average phonon frequency Θ higher than 1200 K, which is the phonon frequency found from the electron-phonon contribution to the energy shift with temperature. Furthermore, the terms Γ_1 and Γ_L in Eqs. (10) and (11) describe the zero-point broadening and additional temperature-independent mechanisms. We have found that the zero-point broadening in diamond is about 150 meV and the largest broadening values in the whole temperature range do not exceed it by more than 30%.

C. Differences in the temperature dependence of diamonds IIa and IIb

The values presented in Tables I and II are the best fits, Eqs. (9)–(11), of the energy and broadening parameters, respectively, which resulted from the $\epsilon(\omega)$ fittings according to Eq. (1). The observed differences in the E_B , E_L , λ , Γ_1 , and Γ_0 values between the two diamond types could be either due to impurities and surface scattering or strain in the materials. The isotope effect^{21,54} is not so important in diamond as in Si and Ge,⁵⁴ because the concentration of ^{13}C is very limited (about 1%). For example, an energy difference of 14 meV was found²¹ for the indirect gap of diamond when the isotope composition changes from ^{12}C to ^{13}C , in quite good agreement with the calculated 17 meV in Ref. 54. Moreover, in Ref. 54 the predicted energy difference for the first direct gap of diamond was calculated at about 22 meV. It should be noted that the scattering of the experimental points at high temperatures in the energy and broadening values of diamond IIb could have a contribution to the observed differences between the two diamond samples.

In order to investigate the presence of strain in diamond we utilized crossed-polarizer optical microscopy (OM). When one examines with crossed-polarizer OM an isotropic sample the field of view will be dark, while in optically anisotropic, birefringent materials it may appear bright. Therefore, if there is any residual strain in the diamond samples, the field of view will appear bright. The examination of the diamond samples IIa and IIb showed large anisotropy for sample IIa and a small one for sample IIb. These observations suggest that there exists residual strain, especially in sample IIa. Rotation of the samples around the light propagation axis revealed a nonuniform strain distribution for the diamond sample IIa, while an almost uniform strain distribution appears in the diamond sample IIb. Similar results were observed in photoelastic measurements of diamond samples in Ref. 55. These residual strains can be related to the samples' history and could be due either to permanent lattice dislocations and stacking faults or twins. Furthermore, these strains could explain⁵⁶ the energy difference of 10–30 meV observed between the first direct gap of the two samples and shown in Figs. 6 and 7. On the other hand, such nonuniform strains could cause an increase in the broadening of the interband transitions. Thus the larger broadenings observed in Figs. 8 and 9 for diamond IIa could be explained by the presence of the nonuniform strains found in this sample.

The presence of surface roughness could change the specular reflection properties of surfaces through two physical effects; first, because part of the incident light is scattered away from the specular direction and second, because part of it may be converted into surface plasmon excitations. However, owing to the fact that (a) we have not observed with the OM technique large differences in the surface quality of the samples, with the sample IIb to be better, (b) the energy range of our measurements was far from the surface-polariton generation energy of diamond, and (c) we have not found differences in the absolute values of the dielectric function in the whole energy

range, we suppose that surface roughness is not responsible for the observed differences.

In the case of Si and Ge (Refs. 57 and 58) it was found that an impurity concentration of about 10^{19} atoms/cm³ causes a redshift in the energy position of the interband transitions E_1 and E_2 and an increase of their broadenings, whenever the crystal lattice contains a *p*- or *n*-type impurity. Thus the presence of impurities could be another cause for the differences between the two samples, because natural diamonds always contain some kind of impurity. In most cases of insulating diamonds this impurity is nitrogen atoms,⁵⁹ while in the semiconducting *p*-type diamond it is boron.^{59,60} Type IIa contains nitrogen aggregates as the major impurity at very low concentration and is considered "clean," with the carriers being electrons. Type IIb is the semiconducting diamond, which exhibits *p*-type conductivity. The impurity concentration N_a ranges normally from 10^{15} – 10^{17} atoms/cm³. Even though we expected the first direct gap of diamond to be more sensitive than the E_1 and E_2 gaps of Si and Ge, the broadening values that we have found for diamond IIb are smaller than those of diamond IIa. Therefore the observed differences between the two samples cannot be attributed to the presence of impurities. Consequently, of the two potential causes of the different behavior of diamonds IIa and IIb, mainly the nonuniform strains observed in diamond IIa seem to be responsible for the differences in E , Γ , and their temperature dependence. However, this statement cannot be generalized for every IIa and IIb natural diamond, since each sample has its own growth history, which influences its impurities and structural-defect concentration.

VI. CONCLUSION

In this work we performed on diamond band-structure calculations, theoretical calculations of the $\epsilon(\omega)$, and temperature-dependent SE measurements using synchrotron radiation. The band-structure calculations using the

LMTO method have shown that the first direct gap of the material is a complex contribution of various band-to-band transitions which take place in the vicinity of the Γ point. Contrary to other III-V compounds, the 3→6 and 4→6 transitions have an early onset and contribute to the fundamental gap. The SE measurements located the gap energy at about 7.1 eV and have shown no structure at energies around 6.5 and 7.5 eV, where earlier experimental results located the first direct gap of diamond and a reflectivity peak, respectively. The derivative analysis of the obtained dielectric-function spectra shows that the first direct gap of diamond is a complex structure and thus better described by a 2D saddle point. The temperature dependence of its energy position and broadening are in very good agreement with published theoretical results and qualitatively similar to the other group-IV and III-V materials, although smaller energy shifts and weaker broadening dependence was found in comparison with the above materials. The observed differences in the energy position, energy shift, and broadening versus temperature of the diamonds IIa and IIb are qualitatively discussed and found to be mainly due to nonuniformities in the strain distribution. The effect of surface oxidation of diamond has also been discussed. Annealing of diamond samples can provoke the reduction of the surface overlayer thickness and improve the measured dielectric-function spectra.

ACKNOWLEDGMENTS

Part of this work was supported by the EC/LSI Program [Contract No. GE 1-0018-D(B)]. The diamond samples used were kindly given to us by E. Anastassakis. We would like to thank M. Cardona for stimulating discussions concerning the temperature-dependence differences of the diamond samples. Also, we would like to thank R. L. Johnson for his support with the UHV ellipsometer and S. Bouladakis for his help on data analysis programs.

- ¹T. Inuzuka, S. Koizumi, and K. Suzuki, in *Diamond and Related Materials*, edited by R. Messier (Elsevier, Amsterdam, 1992), Vol. 1, p. 175.
- ²A. Rengan, N. Biunno, J. Narayan, and P. Moyer, in *Diamond, Silicon Carbide and Other Related Wide Band Gap Semiconductors*, edited by J. T. Glass, R. Messier, and N. Fujimori, MRS Symposia Proceedings No. 162 (Materials Research Society, Pittsburgh, 1990), p. 185.
- ³W. Saslow, T. K. Bergstresser, and M. L. Cohen, *Phys. Rev. Lett.* **16**, 354 (1966).
- ⁴L. Hemstreet, C. Y. Fong, and M. L. Cohen, *Phys. Rev. B* **2**, 2054 (1970).
- ⁵R. Chaney, C. Lin, and E. E. Lafon, *Phys. Rev. B* **3**, 459 (1971).
- ⁶G. S. Painter, D. E. Ellis, and A. R. Lubinsky, *Phys. Rev. B* **4**, 3610 (1971).
- ⁷J. R. Leite, B. I. Bennett, and F. Herman, *Phys. Rev. B* **12**, 1466 (1975).
- ⁸A. Zunger and A. J. Freeman, *Phys. Rev. B* **15**, 5049 (1977).
- ⁹J. R. Chelikowsky and S. G. Louie, *Phys. Rev. B* **29**, 3470 (1984).
- ¹⁰M. Cardona and N. E. Christensen, *Solid State Commun.* **58**,

421 (1984).

- ¹¹H. R. Phillip and E. A. Taft, *Phys. Rev.* **127**, 159 (1962).
- ¹²W. C. Walker and J. Osantowski, *Phys. Rev.* **134**, A153 (1964).
- ¹³C. D. Clark, P. J. Dean, and P. V. Harris, *Proc. R. Soc. London, Ser. A* **277**, 312 (1964).
- ¹⁴H. R. Phillip and E. A. Taft, *Phys. Rev.* **136**, A1445 (1964).
- ¹⁵J. C. Phillips, *Phys. Rev.* **139**, A1291 (1965).
- ¹⁶B. A. Roberts, D. M. Roessler, and W. C. Walker, *Phys. Rev. Lett.* **17**, 302 (1966).
- ¹⁷B. A. Roberts and W. C. Walker, *Phys. Rev.* **161**, 730 (1967).
- ¹⁸J. Fontanella, R. L. Johnson, J. H. Colwell, and C. Andeen, *Appl. Opt.* **16**, 2949 (1977).
- ¹⁹F. J. Himpsel, J. F. van der Veen, and D. E. Eastman, *Phys. Rev. B* **22**, 1967 (1980).
- ²⁰H. Armon and J. P. F. Sellschop, *Phys. Rev. B* **26**, 3289 (1982).
- ²¹A. T. Collins, S. C. Lawson, G. Davies, and H. Kanda, *Phys. Rev. Lett.* **65**, 891 (1990).
- ²²M. Cardona, *Modulation Spectroscopy* (Academic, New York, 1969).

- ²³C. W. Higginbotham, M. Cardona, and F. H. Pollak, *Phys. Rev.* **184**, 821 (1969).
- ²⁴S. Adachi, *Phys. Rev. B* **35**, 7454 (1987).
- ²⁵R. L. Johnson, J. Barth, M. Cardona, D. Fuchs, and A. M. Bradshaw, *Nucl. Instrum. Methods Phys. Res. A* **290**, 606 (1990).
- ²⁶P. G. Lurie and J. M. Wilson, *Surf. Sci.* **65**, 453 (1977).
- ²⁷M. Alouani, L. Brey, and N. E. Christensen, *Phys. Rev. B* **37**, 1167 (1988).
- ²⁸O. Jepsen and O. K. Andersen, *Solid State Commun.* **9**, 1763 (1971); G. Lehman and M. Taut, *Phys. Status Solidi* **54**, 469 (1972).
- ²⁹Y. Petroff, M. Balkanski, J. P. Walter, and M. L. Cohen, *Solid State Commun.* **7**, 459 (1968).
- ³⁰P. Lautenschlager, M. Garriga, S. Logothetidis, and M. Cardona, *Phys. Rev. B* **35**, 9174 (1987).
- ³¹A. Savitzky and J. E. Golay, *Anal. Chem.* **26**, 1627 (1964); J. Steiner, Y. Termonia, and J. Deltour, *ibid.* **44**, 1906 (1972).
- ³²A. D. Papadopoulos and E. M. Anastassakis, *Phys. Rev. B* **43**, 5090 (1991).
- ³³D. F. Edwards and H. R. Phillip, in *Handbook of Optical Constants of Solids*, edited by E. D. Palik (Academic, London, 1985), p. 665.
- ³⁴S. Logothetidis, M. Alouani, M. Garriga, and M. Cardona, *Phys. Rev. B* **41**, 2959 (1991).
- ³⁵S. Logothetidis, *J. Appl. Phys.* **65**, 2416 (1989).
- ³⁶P. Lautenschlager, P. B. Allen, and M. Cardona, *Phys. Rev. B* **33**, 5501 (1986).
- ³⁷Y. Toyozawa, M. Inoue, T. Inui, M. Okazaki, and E. Hamamura, *J. Phys. Soc. Jpn. Suppl.* **21**, 133 (1966).
- ³⁸J. C. Phillips, *Surf. Sci.* **40**, 459 (1973).
- ³⁹E. Gaigher and W. S. Verwoerd, *Surf. Sci.* **103**, 338 (1971).
- ⁴⁰M. L. Cohen, *Phys. Rev. B* **22**, 1095 (1980).
- ⁴¹S. Matsumoto, H. Kanda, Y. Sato, and N. Setaka, *Carbon* **15**, 299 (1977).
- ⁴²B. B. Pate, *Surf. Sci.* **165**, 83 (1986).
- ⁴³R. Jones and T. King, *Philos. Mag. B* **47**, 481 (1983).
- ⁴⁴Y. P. Varshni, *Physica (Utrecht)* **34**, 149 (1967).
- ⁴⁵L. Viña, S. Logothetidis, and M. Cardona, *Phys. Rev. B* **30**, 1979 (1984).
- ⁴⁶P. Lautenschlager, M. Garriga, L. Viña, and M. Cardona, *Phys. Rev. B* **36**, 4821 (1987).
- ⁴⁷S. Logothetidis, M. Cardona, and M. Garriga, *Phys. Rev. B* **43**, 11 950 (1991).
- ⁴⁸P. Lautenschlager, M. Garriga, and M. Cardona, *Phys. Rev. B* **36**, 4813 (1987).
- ⁴⁹S. Logothetidis, L. Viña, and M. Cardona, *Phys. Rev. B* **31**, 947 (1985).
- ⁵⁰P. B. Allen and V. Heine, *J. Phys. C* **9**, 2305 (1976).
- ⁵¹P. B. Allen and M. Cardona, *Phys. Rev. B* **23**, 1495 (1981); **24**, 7479 (1981); **27**, 4760 (1983).
- ⁵²M. Cardona and S. Gopalan, in *Progress in Electron Properties of Solids*, edited by R. Girlanda (Kluwer, Dordrecht, The Netherlands, 1989), p. 51.
- ⁵³S. Gopalan, P. Lautenschlager, and M. Cardona, *Phys. Rev. B* **35**, 5577 (1987).
- ⁵⁴S. Zollner, M. Cardona, and S. Gopalan, *Phys. Rev. B* **45**, 3376 (1992).
- ⁵⁵A. D. Papadopoulos and E. Anastassakis, *Phys. Rev. B* **43**, 9916 (1991).
- ⁵⁶F. H. Pollak and M. Cardona, *Phys. Rev.* **172**, 816 (1968).
- ⁵⁷L. Viña and M. Cardona, *Phys. Rev. B* **29**, 6739 (1984).
- ⁵⁸L. Viña and M. Cardona, *Phys. Rev. B* **34**, 2586 (1986).
- ⁵⁹A. T. Collins, in *Diamond, Silicon Carbide and Other Related Wide Band Gap Semiconductors*, edited by J. T. Glass, R. Messier, and N. Fujimori, MRS Symposia Proceedings No. 162 (Materials Research Society, Pittsburgh, 1990), p. 3.
- ⁶⁰V. S. Vavilov and E. A. Konorova, *Usp. Fiz. Nauk* **118**, 611 (1976) [*Sov. Phys. Usp.* **19**, 301 (1976)].